RSC Advances

ROYAL SOCIETY OF CHEMISTRY

www.rsc.org/advances

Graphical Abstract

Reduced graphene oxide (RGO) in situ composites with cobalt sulfide (CoS) is achieved through a facile hydrothermal approach, and RGO/CoS presents a high specific capacitance of 1130 F g^{-1}.

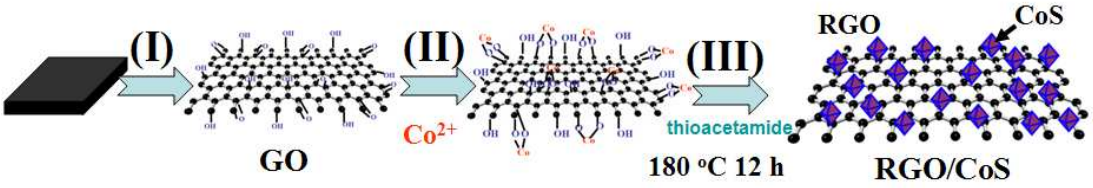

Cite this: DOI: 10.1039/c0xx00000x

www.rsc.org/xxxxxx

ARTICLE TYPE

Facile synthesis of reduced graphene oxide/cobalt sulfide hybrid and its electrochemical capacitance performance

Kai Dai,[a] Dongpei Li,[a] Luhua Lu,*[b] Qi Liu,*[c] Jiali Lv[a] and Guangping Zhu[a]

Received (in XXX, XXX) Xth XXXXXXXXX 20XX, Accepted Xth XXXXXXXXX 20XX

DOI: 10.1039/b000000x

In this work, reduced graphene oxide (RGO) in situ composites with cobalt sulfide (CoS) is achieved through a facile hydrothermal approach. Morphology and structure of the composite materials have been investigated by using scanning electron microscopy (SEM), transmission electron microscopy (TEM), X-ray photoelectron spectra (XPS) and X-ray diffraction (XRD). The results have shown that the composites consist of CoS nanoparticles with the diameter of 30~50 nm uniformly disperse on the basal plane of RGO. The maximum specific capacitances of 1130 F g^{-1} measured by chronopotentiometry at a current density of 0.5 A g^{-1} are obtained in a 6 M KOH aqueous solution, which is 2.4 times higher than that of pure CoS nanoparticle electrodes (473 F g^{-1}). Furthermore, RGO/CoS nanocomposite exhibits good cycling stability with 92.1% capacitance retention over 1000 cycles.

1. Introduction

With the ever-increasing energy and power consumption in applications ranging from portable electronic tools to vehicle electrification and large industrial equipment, intense research efforts have been devoted in developing the technologies for energy conversion and storage, which require high power uptake or delivery and a long cycle life.[1] Of the various power source devices, electrochemical capacitors (ECs), also known as the ultracapacitors or supercapacitors, have received great interest for the satisfying future renewable energy technologies because of their excellent properties such as cheap, high power, effective, environmentally friendly, long cyclic life and fast charge-discharge rates.[2]

Over the past decade, nanostructured metal sulfides have been extensively investigated as electrode materials for EC design because the good performance provided by redox reactions of electrode usually take place in metal sulfides where metal ions have multiple valence states. Sb_2S_3,[3] In_2S_3,[4] $Cu_{2-x}S$,[5] MoS_2,[6] CoS,[7] Bi_2S_3,[8] KCu_7S_4,[9] and Ni_3S_2[10] nanoparticles are widely used in ECs or rechargeable lithium batteries. Among them, CoS has been studied for its relative low-cost, excellent capacitances, low toxicities and large surface sizes than other materials.[11] Nevertheless, CoS nanoparticle does not deliver ideal specific capacitance for its poor electrical conductivity and poor cycling stability.[12] Accordingly, improving electrochemical capacitance substantially to meet the requirements of future practical applications and advancing our understanding of the electrochemical interfaces by developing composite materials at the nanoscale are urgently desirable.

Currently, carbonaceous materials, such as carbon nanotubes,[13] activated carbon,[14] carbon aerogels,[15] activated carbon nanofibers,[16] and template carbon foams,[17] etc., have been frequently chosen as a component for EC materials of effectively improved electrical conductivity and electrochemical stability. Graphene, a two-dimensional nanosheet of graphite, has recently received rapidly growing attention in ECs as it possesses superior electron transport capabilities, a high theoretical surface area (2630 m^2/g), excellent mechanical flexibility, high thermal and chemical stability, and easy functionalization make graphene good substrate to produce graphene-based functional composites.[18] In recent years, many studies covering graphene and related materials used for EC materials have been published. For example, Chidembo et al. reported the capacitances of reduced graphene oxide (RGO) with Co_3O_4 or NiO nanocomposites are 687 F g^{-1} and 656 F g^{-1},[19] which are much higher than that of Co_3O_4 or NiO. Chen et al. obtained hybrid nanostructures of MnO_2/graphene nanosheets for high-performance supercapacitor.[20] Qu et al. have initially shown that the composite of β-CoS nanoparticles decorated graphene has attractive energy storage performance.[21] For the promising energy storage performance that other composites seldom achieved, detailed investigating structure character and understanding performance variation mechanism of metal sulfide and graphene composite structure is important.

In this work, we detailed investigated uniform RGO/CoS nanocomposite formation in aqueous solution via hydrothermal

[a] *College of Physics and Electronic Information, Huaibei Normal University, Huaibei, 235000, P.R. China.*
[b] *State Key Lab of Advanced Technology for Materials Synthesis and Processing, Wuhan University of Technology, Wuhan, 430070, P.R. China. Email address: lhlu@whut.edu.cn*
[c] *Laboratory of Nano-Fabrication and Novel Devices Integrated Technology, Institute of Microelectronics, Chinese Academy of Sciences, Beijing, 100029, P.R. China. Email address: liuqi@ime.ac.cn*

reaction. Electrochemical cyclic voltammeter and galvanostatic charge discharge measurement in combined with porous structure analysis and EIS analysis have been done to understand the mechanism of electrochemical energy performance variation of RGO/CoS nanocomposite in compared with pure CoS.

2. Experimental

2.1 Materials

Natural graphite powder (325 mesh), acetylene black and polytetrafluoroethene (PTFE) was commercially obtained from Alfa-Aesar. Hydrochloric acid (37 %, HCl), concentrated sulfuric acid (98 %, H_2SO_4), potassium hydroxide (KOH) and potassium permanganate ($KMnO_4$) were purchased from Shanghai Chemical Reagent Co., Ltd (P.R. China). Sodium nitrate ($NaNO_3$), ethylene glycol, potassium persulfate ($K_2S_2O_8$), phosphorus pentoxide (P_2O_5), hydrogen peroxide (30 %, H_2O_2), thioacetamide and cobaltous nitrate ($Co(NO_3)_2$•$6H_2O$) were purchased from Sinopharm Chemical Reagent Corp (P.R. China). All reactants were used as raw materials without further purification. Double distilled water was used during the experimental process. The experiments were carried out at room temperature and humidity.

2.2 Preparation of GO

GO was prepared by modified Hummers' method.[22] In detail, 3.2 g graphite was put into a mixture of 15 mL H_2SO_4, 2.5 g $K_2S_2O_8$, and 2.5 g P_2O_5. The solution was heated to 80 °C and kept stirring for 5 h in oil bath. Then the mixture was diluted with 700 mL water, and the product was obtained by filtering using 0.2 μm Nylon film and dried under room temperature. Thereafter, 15.0 g $KMnO_4$ was slowly added with magnetic stirring, to prevent the temperature of the mixture from exceeding 10 °C by ice bath. Then ice bath was then removed and the mixture was stirred at 35 °C for 2 h. The reaction was terminated by adding 800 mL of water and 25 mL H_2O_2 solution. Finally, the GO was obstained by filtration and drying.

2.3 Synthesis of RGO/CoS composite

1.2 g $Co(NO_3)_2 \cdot 6H_2O$, 0.34 g thioacetamide, 1.0 g PVP, 40 µl HCl and 0.03 g GO were initially dissolved in 20 mL water and 20 mL ethylene glycol and ultrasonicated for 1 h. And then, the mixture was further transferred into a 50 mL Teflon-lined autoclave and subsequently heated at 180 °C for 12 h. When it cooled down to room temperature naturally, the RGO/CoS nanocomposites were harvested by centrifugation and washed with water, and were finally dried at 60 °C for 6 h. The weight ratio of CoS in the composite is 93%.

2.4 Characterization

X-ray diffraction (XRD) patterns of CoS and RGO/CoS were carried out using a Rigaku D/MAX 24000 diffractometer with Cu Kα radiation (λ=1.54056Å) and a scanning speed of 0.02 °/s in the 2θ range from 5° to 60°. The accelerating voltage and emission current were 40 kV and 40 mA, respectively. The morphologies of CoS and RGO/CoS were checked using a scanning electron microscopy (SEM, JSM-6700F) at an accelerating voltage of 30 kV equipped with an Inca energy dispersive spectrometer (EDS). The fine structure of the RGO/CoS composite was further investigated on a Tecnai G2 F20 S-Twin transmission electron microscope (TEM) with an accelerating voltage of 200 kV. Core level analysis of the RGO/CoS composite was conducted on an X-ray photoelectron spectrum (XPS) using a Kratos AXIS Ultra DLD X-ray photoelectron spectrometer at room temperature with 1486.6 eV X-ray from the Al Kα line. The Brunauer-Emmett-Teller (BET) specific surface area values were determined by using N_2 adsorption data at 77 K obtained by a Micromeritics ASAP 2010 system with multipoint BET method.

2.5 Electrochemical Measurements

The electrochemical experiments were carried out by a three-electrode system at room temperature on a computer-controlled Shanghai Chenhua CHI 660D workstation. The working electrodes were fabricated by mixing15 wt% acetylene black, 80 wt.% active materials and 5 wt% PTFE binder. Afterward, the mixture was diluted with a small amount of deionized water to form homogeneous mixture slurry. After a short period of drying by evaporation, 5 mg resulting paste was pressed into 10mm × 10mm nickel grid under a pressure of 1.2×10^7 Pa for 30 min. The electrode was then dried for 6 h at room temperature. The electrochemical tests were carried out using 6 M KOH aqueous solution as electrolyte. Before the measurements, the CoS-based electrodes were soaked in 6 M KOH aqueous solution for 10 h. A platinum foil and a saturated calomel electrode (SCE) were used as the counter and reference electrodes, respectively. The galvanostatic charge-discharge process was carried out with different current densities. The specific capacitance (C [F g^{-1}]) of the electrode materials were calculated from the discharge curve according to the following equations:[23]

$$C = I\Delta t / (\Delta V m) \qquad (1)$$

Where: I is the discharge current (A); Δt is the discharge time (s); ΔV is the voltage change (V), excluding the IR drop in the discharge process; and m is the mass of the working electrode material (g), excluding the binder and conductive acetylene black.

3. Results and Discussion

Fig.1 present the designed formation processes for obtaining RGO/CoS nanocomposites. At the stage (I), the sufficient exfoliation of the graphite into GO nanosheets in water, GO nanosheets have their basal planes decorated mostly with epoxy and hydroxyl groups, while carbonyland carboxyl groups are located at the edges by the modified Hummers' method. These functional groups enable the subsequent in situ formation of nanostructures attaching on the surfaces and edges of GO nanosheets. At the stage (II), Co^{2+} ions, formed by the dissolution of $Co(NO_3)_2 \cdot 6H_2O$, favorably bind with the O atoms of the negatively charged oxygen-containing functional groups on GO sheets via an electrostatic attraction. At the stage (III), with the help of thioacetamide under condition of 180 °C, large number of CoS nuclei were formed in a short time from the redox reaction

occurring between Co^{2+} and H_2S. The chemical reaction involved in the growth of CoS is according to the following equations:

$$CH_3CSNH_2 + H_2O \xrightarrow{H^+} CH_3CONH_2 + H_2S \quad (2)$$

$$Co^{2+} + H_2S \rightarrow CoS\downarrow + 2H^+ \quad (3)$$

$$CH_3CONH_2 + H_2O \xleftrightarrow{H^+} CH_3COONH_4 \quad (4)$$

The CoS molecules may form bonds with O atoms of the functional groups via an intermolecular hydrogen bond or a covalent coordination bond, acting as anchor sites for the crystals growth, and the strong chemical and/or physical absorption of CoS nanocrystals on GO nanosheets after the hydrothermal reaction, and at the same time, GO was reduced to RGO.

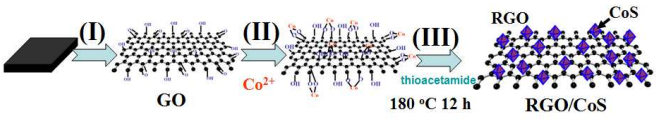

Fig.1. Illustration of three steps for RGO/CoS nanocomposite formation. (I) exfoliation of graphite oxide into GO sheets, (II) formation of Co nuclei and interaction between GO sheets and Co^{2+} through hydrogen bonding, (III) hydrothermal treatment at 180 °C for 12 h to produce RGO/CoS composite

Fig.2 shows the XRD patterns of GO, CoS and RGO/CoS composites, respectively. For GO, the XRD peak at 10° for the (001) facets corresponds to 0.87 nm interlayer spacing, which is much larger than that of pristine graphite (0.34 nm) due to the introduction of oxygen-containing functional groups on the graphite sheets.[24] The diffraction angles at 2θ = 30.62°, 35.50°, 47.02° and 54.86°, can be assigned to (1 0 0), (1 0 1), (1 0 2) and (1 1 0) crystal planes of pure CoS with the hexagonal structures and the lines match well with the value reported by JCPDS (No. 75-0605, a=0.338 nm and c=0.515 nm).

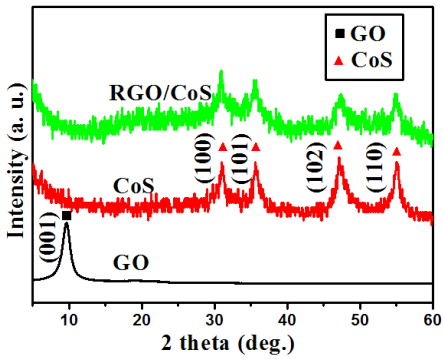

Fig.2. XRD patterns of GO, CoS and GO/CoS composites

Fig.3a and 3b show the typical SEM images of CoS and RGO/CoS composites, respectively. The size of the as-synthesized CoS nanoparticles was ca. 30~50 nm, and the RGO sheets and the nanostructures of CoS particles can be observed, signifying the successful incorporation of CoS nanoparticles onto RGO sheets for a composite. Fig.3c and 3d show the EDS spectra of CoS and RGO/CoS composites, respectively. The pattern indicates that CoS crystals only contain elements of Co and S, without any other impurities, and the as-synthesized RGO/CoS composites only contain elements of C, Co, S and O. Fig.3e and 3f show the typical TEM images of GO and RGO/CoS composites, respectively. The binding between RGO and CoS surfaces was tight enough to resist repeated rinsing and ultrasonication.

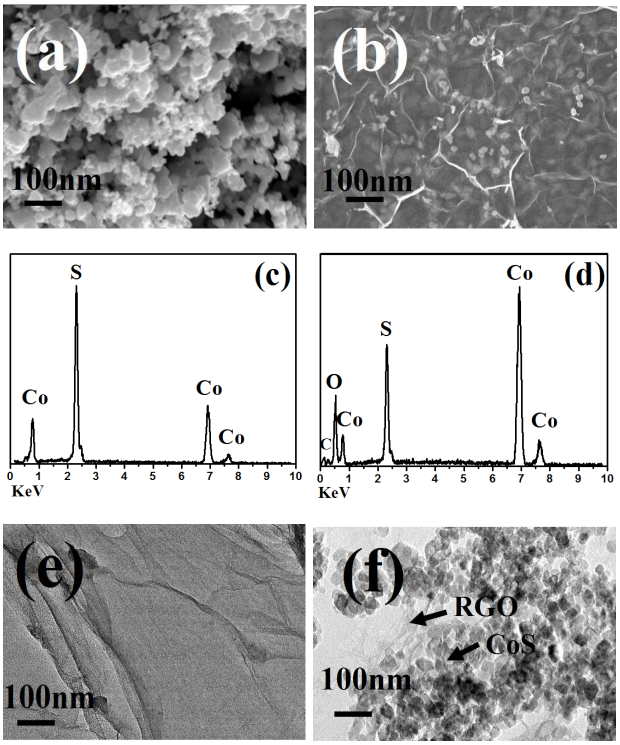

Fig.3. SEM images of (a) CoS and (b) RGO/CoS composites, EDS spectra of (c) CoS and (d) RGO/CoS composites and TEM images of (e) GO and (f) RGO/CoS composites

The XPS spectrum including signals for C1s, Co2p, O1s and S2p of RGO/CoS composites to probe the chemical environment of the elements in the near surface range has shown in Fig.4a. As indicated in Fig.4b, the asymmetrical and broad features of the observed C1s peaks suggest the co-existence of distinguishable models. Deconvolution core level spectra at about 284.82, 286.88 and 288.72 eV have been giving. The sharp peak located at 284.82 eV is attributed to sp^2-hybridized carbons (C-C).[25] While the peak at 286.88 eV is ascribed to the existence of C-OH bonds,[26] and the relatively weak peak at 288.72 eV is ascribed to the existence of C-OOH bonds.[27] Fig.4c shows the high-resolution spectra of O1s. In the case of RGO/CoS nanocomposite, the curve fitting of O1s spectrum basically indicates two components centered at 529.44 and 531.42 eV, which are commonly ascribed to the the surface oxygen complexes of carbon phase.[28] Fig.4d shows the high-resolution spectra of Co2p, the peaks at 794.24 and 779.16 eV correspond to the Co2p1/2 and Co2p3/2 spin-orbit peaks of CoS,[29] and a broadened peak at 800.26 eV can be attributed to satellite signal. As indicated in Fig.4e, the peak centered at 162.1 eV corresponds with the binding energies of Co-S.[30]

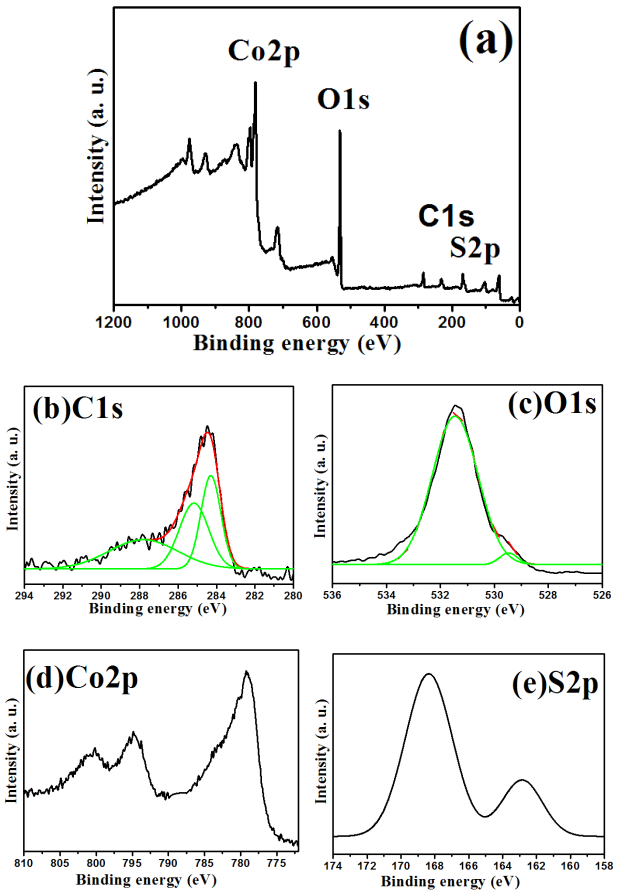

Fig.4. The overview(a) and the corresponding high-resolution XPS spectra (b) C1s, (c) O1s, (d) Co2p and (e) S2p of RGO/CoS composites

To enhance the utilization of EC material for achieving high capacitance, it is vital to design material structures with large surface areas for efficient access of electrolyte ions. Fig.5 shows the N_2 adsorption-desorption isotherms for CoS and RGO/CoS nanocomposites at 77 K. The data of BET surface area, pore specific volume of samples are listed in Table. 1. The N_2 sorption isotherm for the RGO/CoS sample displays hysteresis loops at relative pressures (P/P_0) close to unity, indicating the presence of large mesopores and macropores. Table.1 shows that RGO/CoS composite samples have much larger specific surface areas than pure CoS. This is due to the presence of RGO in the composites, which has an extremely high surface area.

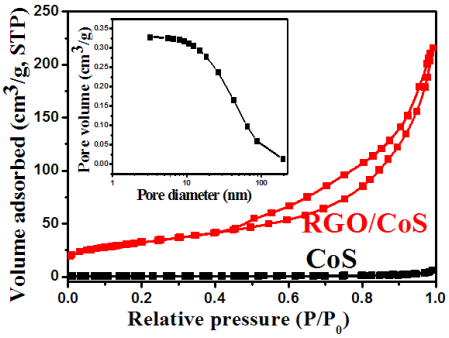

Fig.5. Isotherms for Nitrogen adsorption-desorption of CoS and RGO/CoS composites (Inset: pore size distribution of RGO/CoS)

Table.1 BET surface area and pore volume data of as-prepared samples

Samples	BET surface area ($m^2.g^{-1}$)	Total pore volume ($cm^3.g^{-1}$)
CoS	1.4	0.009
RGO/CoS	92.6	0.143

Fig.6a and 6b present the cyclic voltammetry (CV) curves of CoS and RGO/CoS electrodes within the electrochemical window from -0.1 to 0.6 V under the scan rate of different potential scan rates ranging from 1 to 50 mV s^{-1}. The two anodic peaks are likely due to the oxidations of CoS to CoSOH and CoSOH to CoSO, separately:[31]

$$CoS + OH^- \rightleftharpoons CoSOH + H_2O + e^- \quad (5)$$

$$CoSOH + OH^- \rightleftharpoons CoSO + H_2O + e^- \quad (6)$$

The two oxidized peaks of the as-prepared CoS nanomaterial and RGO/CoS composite occur separately at range of 0.1-0.2 V and 0.4-0.5 V. Scan rate and the shape and the structure of electrode material will influence the redox peaks.[29, 32] The current CV density of CoS-based materials gradually increased with the increase of scan rate, RGO/CoS electrode yields the largest current and results in much higher capacitance. The reasons can be explained as the follows: (a) the synergistic effects from RGO and CoS nanoparticle of composite electrodes that further boosts the electrical conductivity and contributes the redox-based pseudocapacitance; (b) the charge-discharge process of RGO/CoS composite in the KOH aqueous electrolyte was mainly governed by the insertion of ions from the electrolyte into almost all available area of the electrode and its release to the electrolyte, which can be facilitated by the special 2-dimensional structure.

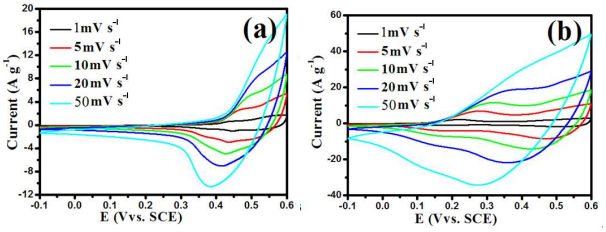

Fig.6. CV curves of (a) CoS and (b) RGO/CoS composite at different scan rate

Galvanostatic charge-discharge measurements were also carried out to assess the potential of RGO/CoS composite as electrode materials for ECs. Fig.7a and 7b show the charge-discharge curves for the synthesized CoS and RGO/CoS at varied current densities (from 0.5 A g^{-1} to 5 A g^{-1}) within a voltage range between 0.0 and 0.5 V, respectively. According to equation (1), the corresponding specific capacitances of CoS and RGO/CoS composites are shown in Fig.7c. The theoretical capacity of CoS is about 1300 F g^{-1},[33] but CoS nanoparticles can not deliver ideal specific capacitance because of the poor electrical conductivity. RGO/CoS composite exhibits the maximum specific capacitance of 1130 F g^{-1} at 0.5 A g^{-1}, which is 2.4 times that of pure CoS

nanoparticles (473 F g^{-1}). The coulombic efficiency (CE) were calculated by discharge capacity/charge capacity, CE is 92%, 88%, 74% and 64% for CoS at 0.5 A g^{-1}, 1 A g^{-1}, 3 A g^{-1} and 5 A g^{-1}, respectively, and 97%, 92%, 87% and 80% for RGO/CoS at 0.5 A g^{-1}, 1 A g^{-1}, 3 A g^{-1} and 5 A g^{-1}, respectively. Thus, CoS effectively attaches to the surfaces of conductive RGO can effectively make its intrinsic electrochemical capacitance well embodied. Moreover, RGO supplies sufficient electrochemically active sites for effective redox reactions on the CoS surfaces and provided effective channels for the deep intercalation or de-intercalation of ions, which is beneficial to the fast transfer of ions throughout the whole electrode, consequently improving electrochemical performance.[34] Thus RGO/CoS composite exhibits attractive high specific capacitance because of the synergistic effect of the pseudocapacitive of CoS and high conductive and large surface area of RGO. To understand the electrochemical performance characteristics of RGO/CoS composites, we performed EIS measurements on these samples as well as CoS nanoparticles sample. Fig.7d shows the Nyquist plots obtained from the EIS measurements. The EIS data are fitted based on an equivalent circuit model that consists of a bulk solution resistance R_S, electrode resistance R_e, a charge-transfer resistance R_{ct}, a capacitive element C_{dl}, and a Warburg element (W).[35] Accordingly, R_S is 0.23 Ω, the R_e of the CoS and RGO/CoS is 1.36 and 0.23 Ω, respectively, whereas R_{ct} is 2.12 and 0.22 Ω in the same order. As is well known, the electrochemical capacitor performance is closely related to the charge-transfer resistance R_{ct}. The higher charge-transfer resistance corresponds to the lower specific capacitance. This clearly shows that the RGO/CoS composite displays much more favorable charge-transfer kinetics than CoS. Furthermore, the conducting agent obviously affects the specific capacitance of the EC in the CoS-based electrode.

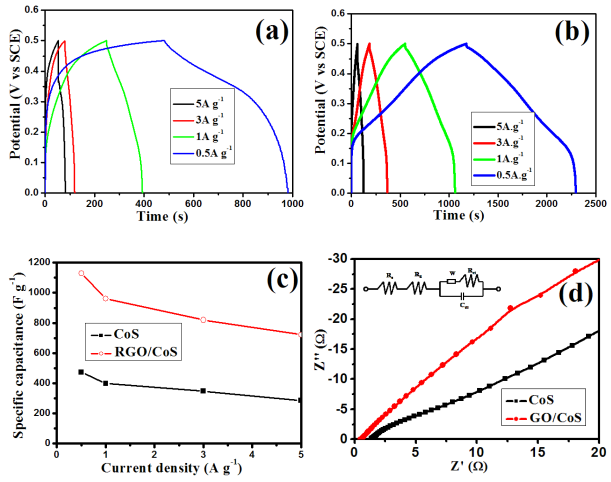

Fig.7. Galvanostatic charge-discharge of (a) CoS, and (b) RGO/CoS at current densities of 0.5, 1.0, 3.0, and 5.0 A g^{-1}, respectively, (c) Variation of specific capacitance against current densities for CoS and RGO/CoS, and (d) EIS Nyquist plots for RGO/CoS and CoS

Fig. 8 shows the electrochemical stability of the RGO/CoS and CoS electrodes in 6M KOH electrolyte by galvanostatic charging-discharging at a current density of 0.5 A g^{-1} within a voltage range of 0.0 and 0.5 V for 1000 cycles. 92.1% of the initial capacitance of RGO/CoS is preserved after 1000 charge-discharge cycles, but CoS nanoparticles only retains 78.2% of initial capacitance after 1000 cycles. The unique structure of RGO/CoS nanocomposite effectively prevents the aggregation of RGO and CoS and consequently provides high specific surface area, which is favorable for fast hydrated ion transport in the electrolyte to the surfaces of both RGO and CoS nanoparticles. Furthermore, the superior electrical conductivity of RGO can significantly decrease the internal resistance of electrode by the construction of a conductive network. CoS nanoparticles with small diameters are also helpful for shortening ion diffusion path, which can greatly reduce the charge transfer resistance and ionic diffusion resistance.[36] This kind of relatively low-cost RGO/CoS nanocomposite combines high capacitance and long cycling life. Therefore, the present RGO/CoS nanocomposite could be designed to meet the demand for EC electrodes.

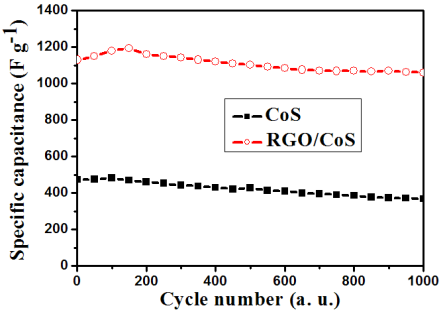

Fig.8. Cycle performance of RGO/CoS and CoS particles measured at a current density of 0.5 A g^{-1}

Conclusions

A promising route for easy and large scale synthesis of RGO/CoS nanocomposite is developed. The CoS nanoparticles with a size of 30~50 nm are uniformly anchored on both sides of the RGO nanosheets. The as-synthesized RGO/CoS nanocomposite exhibits attractive specific capacitance as high as 1130 F g^{-1} at 0.5 A g^{-1} and 92.1% maintenance effect after 1,000 cycles of electrochemical charge-discharge. The improvement in cycling stability is attributed to the introduction of the flexible graphene that not only buffers the volume changes and but also prevents CoS nanoparticles from aggregating. The introduced graphene also offers 2D conductive networks and enhances the charge transfer rate, leading to enhanced rate capability.

Acknowledgments

This work was supported by the National Natural Science Foundation of China (51302101, 21303129), the Natural Science Foundation of Anhui Province (1408085QE78), the key Foundation of Educational Commission of Anhui Province (KJ2012A250), and the Huaibei Science and Technology Development Funds (20110305).

Notes and references

1 M. Armand and J.-M. Tarascon, *Nature*, 2008, **451**, 652; P. Simon and Y. Gogotsp, *Nat. Mater.*, 2008, **7**, 845; X. Yang, C. Cheng, Y. Wang, L. Qiu and D. Li, *Science*, 2013, **341**, 534; Q. Lu, J. G. Chen and J. Q. Xiao, *Angew. Chem. Int. Ed.*, 2013, **52**, 1882; A. S. Aricò, P. Bruce, B. Scrosati, J.-M. Tarascon and W. V. Schalkwijk, *Nat. Mater.*, 2005, **4**, 366.

2 G. Wang, L. Zhang and J. Zhang, *Chem. Soc. Rev.*, 2012, **41**, 797; Q. Lu, M. W. Lattanzi, Y. Chen, X. Kou, W. Li, X. Fan, K. M. Unruh, J. G. Chen and J. Q. Xiao, *Angew. Chem. Int. Ed.*, 2011, **123**, 6979;

L. Zhang, F. Zhang, X. Yang, G. Long, Y. Wu, T. Zhang, K. Leng, Y. Huang, Y. Ma, A. Yu and Y. Chen, *Sci. Rep.*, 2013, **3**, 1408; L. Bao, J. Zang and X. Li, *Nano Lett.*, 2011, **11**, 1215; M. Wu, J. Gao, S. Zhang and A. Chen, *J. Power Sources*, 2006, **159**, 365.
3 B. N. Reddy, M. Deepa and A. G. Joshi, *Phys. Chem. Chem. Phys.*, 2014, 16, 2062.
4 S. Acharya, S. Sarkar and N. Pradhan, *J. Phys. Chem. Lett.*, 2012, **3**, 3812.
5 N. J. Freymeyer, P. D. Cunningham, E. C. Jones, B. J. Golden, A. M. Wiltrout and K. E. Plass, *Cryst. Growth Des.*, 2013, **13**, 4059.
6 K.-J. Huang, L. Wang, Y.-J. Liu, Y.-M. Liu, H.-B. Wang, T. Gan and L.-L. Wang, *Int. J. Hydrogen Energ.*, 2013, **38**, 14027; G. Ma, H. Peng, J. Mu, H. Huang, X. Zhou and Z. Lei, *J. Power Sources*, 2013, **229**, 72.
7 H. Wan, X. Ji, J. Jiang, J. Yu, L. Miao, L. Zhang, S. Bie, H. Chen and Y. Ruan, *J. Power Sources*, 2013, **243**, 396.
8 Z. Zhang, C. Zhou, L. Huang, X. Wang, Y. Qu, Y. Lai and J. Li, *Electrochim. Acta*, 2013, **114**, 88.
9 S. Dai, Y. Xi, C. Hu, J. Liu, K. Zhang, X. Yue and L. Cheng, *J. Mater. Chem. A*, 2013, **1**, 15530.
10 C.-S. Dai, P.-Y. Chien, J.-Y. Lin, S.-W. Chou, W.-K. Wu, P.-H. Li, K.-Y. Wu and T.-W. Lin, *ACS Appl. Mater. Interfaces*, 2013, **5**, 12168.
11 F. Tao, Y.-Q. Zhao, G.-Q. Zhang and H.-L. Li, *Electrochem. Commun.*, 2007, **9**, 1282; G. Huang, T. Chen, Z. Wang, K. Chang and W. Chen, *J. Power Sources*, 2013, **235**, 122; M.-R. Gao, Y.-F. Xu, J. Jiang and S.-H. Yu, *Chem. Soc. Rev.*, 2013, **42**, 2986; J. Pu, Z. Wang, K. Wu, N. Yu and E. Sheng, *Phys. Chem. Chem. Phys.*, 2014, **16**, 785.
12 J.-Y. Lin, Y.-T. Tsai, S.-Y. Tai, Y.-T. Lin, C.-C. Wan, Y.-L. Tung and Y.-S.Wu, *J. Electrochem. Soc.*, 2013, **160**, D46.
13 K. Dai, C. Liang, L. Lu, J. Dai, G. Zhu, Z. Liu, Q. Liu and Y. Zhang, *Mater. Chem. Phy.*, 2014, **143**, 1344.
14 X. Du, C. Wang, M. Chen, Y. Jiao and J. Wang, *J. Phys. Chem. C*, 2009, **113**, 2643.
15 A. Halama, B. Szubzda and G. Pasciak, *Electrochim. Acta*, 2010, **55**, 7501.
16 V. Barranco, M. A. Lillo-Rodenas, A. Linares-Solano, A. Oya, F. Pico, J. Ibañez, F. Agullo-Rueda, J. M. Amarilla and J. M. Rojo, *J. Phys. Chem. C*, 2010, **114**, 10302.
17 Y. Lv, L. Gan, M. Liu, W. Xiong, Z. Xu, D. Zhu and D. S. Wright, *J. Power Sources*, 2012, **209**, 152.
18 D. Chen, L. Tang and J. Li, *Chem. Soc. Rev.*, 2010, **39**, 3157; D. Li, M. B. Muller, S. Gilje, R. B. Kaner and G. G. Wallace, *Nat. nanotechnol.*, 2008, **3**, 101; Y. Zhao, J. Liu, Y. Hu, H. Cheng, C. Hu, C. Jiang, L. Jiang, A. Cao and L. Qu, *Adv. Mater.*, 2013, **25**, 591; X. Zhao, C. M. Hayner, M. C. Kung and H. H. Kung, *Adv. Energy Mater.*, 2011, **1**, 1079; K. Dai, L. Lu, C. Liang, J. Dai, Q. Liu, Y. Zhang, G. Zhu and Z. Liu, *Electrochem. Acta*, 2014, **116**, 111.
19 A. Chidembo, S. H. Aboutalebi, K. Konstantinov, M. Salari, B. Winton, S. A. Yamini, I. P. Nevirkovets and H. K. Liu, *Energy Environ. Sci.*, 2012, **5**, 5236.
20 S. Chen, J. Zhu, X. Wu, Q. Han and X. Wang, *ACS Nano*, 2010, **4**, 2822.
21 B. Qu, Y. Chen, M. Zhang, L. Hu, D. Lei, B. Lu, Q. Li, Y. Wang, L. Chen and Taihong Wang, *Nanoscale*, 2012, **4**, 7810.
22 W.S. Hummers and R.E. Offeman, *J. Am. Chem. Soc.*, 1958, **80**, 1339; Y. Wang, Y. M. Li, L. H. Tang, J. Lu and J. H. Li, *Electrochem. Commun.*, 2009, **11**, 889.
23 C. Guan, X. Li, Z. Wang, X. Cao, C. Soci, H. Zhang and H. J. Fan, *Adv. Mater.*, 2012, **24**, 4186; B. Gao, C. Yuan, L. Su, L. Chen and X. Zhang, *J Solid State Electr.*, 2008, **13**, 1251.
24 Q. Liu, J. Shi, J. Sun, T. Wang, L. Zeng and G. Jiang, *Angew. Chem. Int. Ed.*, 2011, **123**, 6035.
25 R. Bhowmick, S. Rajasekaran, D. Friebel, C. Beasley, L. Jiao, H. Ogasawara, H. Dai, B. Clemens and A. Nilsson, *J. Am. Chem. Soc.*, 2011, **133**, 5580.
26 H. Ago, T. Kugler, F. Cacialli, W.R. Salaneck, M.S.P. Shaffer, A.H. Windle and R.H. Friend, *J. Phys. Chem. B*, 1999, **103**, 8116.
27 K. Dai, G. Dawson, S. Yang, Z. Chen and L. Lu, *Chem. Eng. J*, 2012, **191**, 571.
28 K. Dai, L. Lu, Q. Liu, G. Zhu, Q. Liu and Z. Liu, *Dalton Tran.*, 2014, **43**, 2202.
29 C.-Y. Chen, Z.-Y. Shih, Z. Yang and H.-T. Chang, *J. Power Sources*, 2012, **215**, 43.
30 S.-J. Bao, Y. Li, C. M. Li, Q. Bao, Q. Lu and J. Guo, *Cryst. Growth Des.*, 2008, **8**, 3745.
31 Z. Yang, C.-Y. Chen and H.-T. Chang, *J. Power Sources*, 2011, **196**, 7874.
32 S.-J. Bao, C.M. Li, C.-X. Guo, Y. Qiao, *J. Power Sources*, 2008, **180**, 676.
33 R. D. Apostolova, E. M. Shembel, I. Talyosef, J. Grinblat, B. Markovsky and D. Aurbach, *Russ. J. Electrochem.*, 2009, **45**, 311; A. Débart, L. Dupont, R. Patrice and J. M. Tarascon, *Solid State Sci.*, 2006, **8**, 640; W. Luo, Y. Xie, C. Wu and F. Zheng, *Nanotechnology*, 2008, **19**, 075602; J. M. Yan, H. Z. Huang, J. Zhang, Z. J. Liu and Y. Yang, *J. Power Sources*, 2005, **146**, 264.
34 Y. J. Mai, X. L. Wang, J. Y. Xiang, Y. Q. Qiao, D. Zhang, C. D. Gu and J. P. Tu, *Electrochim. Acta*, 2011, **56**, 2306; M. Zhang, D. Lei, Z. Du, X. Yin, L. Chen, Q. Li, Y. Wang and T. Wang, *J. Mater. Chem.*, 2011, **21**, 1673.
35 H.-Y. Wu and H.-W. Wang, *Int. J. Electrochem. Sci.*, 2012, **7**, 4405; T. Y. Wei, C. H. Chen, K. H. Chang, S. Y. Lu and C. C. Hu, *Chem. Mater.*, 2009, **21**, 3228.
36 C. Jiang, E. Hosono and H. Zhou, *Nanotoday*, 2006, **1**, 28.
37